Atmos. Chem. Phys., 20, 9821–9835, 2020
https://doi.org/10.5194/acp-20-9821-2020

Atmospheric Chemistry and Physics
Open Access
EGU

Probing key organic substances driving new particle growth initiated by iodine nucleation in coastal atmosphere

Yibei Wan[1], Xiangpeng Huang[2], Bin Jiang[3], Binyu Kuang[4], Manfei Lin[4], Deming Xia[5], Yuhong Liao[3], Jingwen Chen[5], Jian Zhen Yu[4], and Huan Yu[1]

[1]Department of Atmospheric Science, School of Environmental Studies, China University of Geosciences, Wuhan, 430074, China
[2]School of Environmental Science and Engineering, Nanjing University of Information Science and Technology, Nanjing, 210044, China
[3]Guangzhou Institute of Geochemistry, Chinese Academy of Sciences, Guangzhou 510640, China
[4]Department of Chemistry, Hong Kong University of Science & Technology, Clear Water Bay, Kowloon, Hong Kong SAR, China
[5]School of Environmental Science and Technology, Dalian University of Technology, Dalian 116024, China

Correspondence: Huan Yu (yuhuan@cug.edu.cn)

Received: 9 April 2020 – Discussion started: 30 April 2020
Revised: 26 June 2020 – Accepted: 15 July 2020 – Published: 21 August 2020

Abstract. Unlike the deep understanding of highly oxygenated organic molecules (HOMs) driving continental new particle formation (NPF), little is known about the organic compounds involved in coastal and open-ocean NPF. On the coastline of China we observed intense coastal NPF events initiated by iodine nucleation, but particle growth to cloud condensation nuclei (CCN) sizes was dominated by organic compounds. This article reveals a new group of $C_{18,30}H_hO_oN_n$ and $C_{20,24,28,33}H_hO_o$ compounds with specific double-bond equivalents and oxygen atom numbers in new sub 20 nm coastal iodine particles by using ultrahigh-resolution Fourier transform–ion cyclotron resonance mass spectrometry (FT-ICR-MS). We proposed these compounds are oxygenated or nitrated products of long-chain unsaturated fatty acids, fatty alcohols, nonprotein amino acids or amino alcohols emitted mutually with iodine from coastal biota or biologically active sea surface. Group contribution method estimated that the addition of $–ONO_2$, –OH and –C=O groups to the precursors reduced their volatility by 2–7 orders of magnitude and thus made their products condensable onto new iodine particles in the coastal atmosphere. Nontarget MS analysis also provided a list of 440 formulas of iodinated organic compounds in size-resolved aerosol samples during the iodine NPF days, which facilitates the understanding of unknown aerosol chemistry of iodine.

1 Introduction

Atmospheric new particle formation (NPF) contributes over half of global cloud condensation nuclei (CCN) (Merikanto et al., 2009) and thus influences cloud properties and Earth's radiation budget (Metzger et al., 2010). By deploying a high-resolution chemical ionization mass spectrometer, recent laboratory and field studies have identified a group of highly oxygenated multifunctional organic molecules (HOMs) with high O/C ratios and low volatility from the reactions of volatile organic compounds (VOCs) such as monoterpenes (Ehn et al., 2014), sesquiterpenes (Richters et al., 2016) and alkenes (Mentel et al., 2015) with a hydroxyl radical (OH), ozone (O_3), nitrate radicals (NO_3) and chlorine atoms (Wang et al., 2020). These HOMs play an important role in particle nucleation and growth of continental NPF, as well as in the formation of secondary organic aerosols.

Unlike the deep understanding of continental HOMs, little is known about the role of organic compounds in the NPF in coastal or open-ocean atmosphere. The current state of knowledge is that the photolysis of molecular iodine (I_2) or iodomethane is the source of iodine oxides or oxoacids, the self-clustering of which could initiate NPF events with a particle number concentration sometimes exceeding $10^6\,cm^{-3}$ (O'Dowd et al., 2002; Saiz-Lopez and

Plane, 2004; Burkholder et al., 2004; Mahajan et al., 2010, 2012; Sipilä et al., 2016; Stevanović et al., 2019; Kumar et al., 2018). But it is unknown if other species are needed to drive the growth of iodine clusters to CCN sizes in coastal or open-ocean atmosphere (Saiz-Lopez et al., 2012). Iodine-induced NPF (I-NPF) events were mostly reported in European coastlines (Yoon et al., 2006; Mahajan et al., 2010) and polar regions (Allan et al., 2015; Roscoe et al., 2015; Dall'Osto et al., 2018). In 2019 we provided evidence of I-NPF in the southeast coastline of China, based on particle number size distribution and iodine measurements (Yu et al., 2019). The focus of that paper (Yu et al., 2019) is, however, the speciation of organic iodine compounds in size-segregated aerosol samples. Moreover, the use of a relatively low-resolution time-of-flight (TOF) mass analyzer and in vitro signal amplification approach in that paper did not allow the detection of the majority of non-aromatic organic iodine compounds. Organic iodine remains the most significant unknown in aerosol iodine chemistry at present (Saiz-Lopez et al., 2012).

Fourier transform ion cyclotron resonance (FT-ICR) coupled with soft ionization techniques such as electrospray ionization (ESI) and ambient pressure chemical ionization (APCI) allows characterization of complex organic mixtures at the molecular level due to its ultrahigh resolution and mass accuracy (Pratt and Prather, 2012). This technique has been used to examine molecular composition of organic aerosols (Schum et al., 2018; An et al., 2019; Zuth et al., 2018; Daellenbach et al., 2019; Xie et al., 2020) and cloud water (Zhao et al., 2013; Bianco et al., 2018). Studies investigating coastal organic aerosols have been rare. Virtually no study reported the characterization of organic compounds driving the growth of coastal or open-ocean new particles.

In this study, comprehensive chemical composition analyses were conducted on the size-segregated aerosol samples down to 10 nm, collected by 13-stage nano-MOUDI (nano-micro-orifice uniform deposit impactor) during the intense I-NPF days at a coastal site in China. Relative abundances of HSO_4^-, total iodine and total organic carbon (TOC) in 10–56 nm particles were compared between the I-NPF days and conventional continental NPF (C-NPF) days. In particular, using ultrahigh-resolution FT-ICR-MS, we conducted a nontarget analysis of particle-phase organic compounds to explore their molecular identity, formation mechanism and the role in new particle growth in the coastal atmosphere.

2 Methodology

2.1 Sampling collection

The sampling site (29°29′ N, 121°46′ E) is near a small fishing village without permanent residents on the coastline of the East China Sea. It can be seen from the aerial photo (Fig. S1a in the Supplement) that from the east to the west are the sea, intertidal zone, small paddy fields and mountain. The sampling site is about 40 and 200 m away at high tide and low tide, respectively. The classification of I-NPF event, C-NPF event or non-NPF was based on particle number size distributions (PNSDs) between 2 and 750 nm monitored from January to May 2018 by a scanning mobility particle spectrometer (SMPS; TSI DMA3081 and CPC3775; scanning range: 40–750 nm) and a neutral cluster air ion spectrometer (NAIS; scanning range: 2–42 nm). A nano-MOUDI sampling scheme was implemented according to the PNSD measurement. One set of nano-MOUDI samples was collected during the C-NPF days from 11 to 13 February; a second set was collected during overcast non-NPF days from 16 to 18 April; a third set was collected during the I-NPF days from 9 to 11 May. The PNSD during the three periods are shown in Fig. S2. Each set of nano-MOUDI samples was collected continuously for 72 h, during which NPF occurred on a daily basis, so that particle chemical composition of different event types can be obtained from offline analyses. Aluminum foil filters were used as sampling substrate to avoid the adsorption of gaseous species. For each set of nano-MOUDI samples, two nano-MOUDIs were placed side by side to collect 10–100 nm particles (on stages 10–13; other stages were silicon greased) and 100 nm–18 µm particles (on stages 1–9) separately, in order to reduce potential positive particle-bounce artifacts. Three additional sets of blank samples were collected by placing a high-efficiency particulate air (HEPA) filter at the gas inlet of the nano-MOUDI. Detailed information on aerosol sample collection could be found in Yu et al. (2019).

2.2 Sample preparation and analysis

Half of each filter was transferred into a 20 mL tapered plastic centrifuge tube, and 10 mL mixed solvent (1 : 1 v/v water and methanol; LCMS grade) is added. The mixture was sonicated for 40 min and filtered by a 0.2 µm PTFE membrane syringe filter. The filtrate was evaporated to almost dryness in a rotary evaporator below 40 °C and subsequently redissolved in 0.5 mL water. After being centrifuged for 30 min at 12 000 rpm, the supernatant was collected for total iodine (I) analysis by Agilent 7500a ICP-MS (Agilent Technologies, Santa Clara, CA, USA) and HSO_4^- analysis by UPLC-ESI-Q-TOF-MS. The measurements of HSO_4^- and total I were elaborated in our previous article Yu et al. (2019). Another half of each filter was extracted in the same way but used for TOC analysis by a TOC analyzer (Model TOC-5000A, Shimadzu, Japan) and nontarget MS analysis of organic compounds (OCs) by ESI-FT-ICR-MS (SolariX XR 9.4T instrument, Bruker Daltonics, Coventry, UK). Samples were infused by a syringe pump and analyzed in both positive (ESI+) and negative (ESI−) modes. ESI-FT-ICR MS operation conditions are included in the Supplement. Field blank sample extracts were analyzed following the same procedure.

2.3 FT-ICR MS data processing

A resolving power ($m/\Delta m_{50\,\%}$) 550 000 at m/z 300 of our FT-ICR-MS allows the determination of possible formulas for singly charged molecular ions. Only m/z values between 150–1000 that satisfy the signal-to-noise (S/N) ratio > 10 were considered. For each m/z value, several scientific rules were applied to calculate a reasonable elemental formula of natural organic molecule: the general formula is $C_{1-50}H_{1-100}O_{0-50}N_{0-10}I_{0-3}$ in the ESI+ mode; elemental ratios H/C, O/C and N/C are limited to 0.3–3, 0–3 and 0–1.3, respectively. The general formula is $C_{1-50}H_{1-100}O_{1-50}N_{0-5}S_{0-2}I_{0-3}$ in the ESI− mode; elemental ratios H/C, O/C, N/C and S/C are limited to 0.3–3, 0–3, 0–0.5 and 0–0.2, respectively. Mass error must be smaller than 0.5 ppm. Formulas containing C, H, O, N, S and I isotopologues were removed from the formula lists. A formula with $m/z > 500$ was not reported if it did not belong to any CH_2 homologous series. For the formula $C_cH_hO_oN_nS_sI_x$, double-bond equivalents (DBEs) defined as $\mathrm{DBE} = \frac{2c+2-h+n-x}{2}$ were required to be nonnegative. Formula calculation was done following the same procedure for the three field blank samples. All formulas found in the field blank samples, regardless of peak intensity, were excluded from the formula lists of real samples. Aromaticity index (AI) is calculated from $\mathrm{AI} = \frac{\mathrm{DBE_{AI}}}{C_{\mathrm{AI}}} = \frac{1+c-o-s-0.5h}{c-o-s-n}$. If $\mathrm{DBE_{AI}} \le 0$ or $C_{\mathrm{AI}} \le 0$, then $\mathrm{AI} = 0$. A threshold value of $\mathrm{AI} \ge 0.5$ provides an unambiguous minimum criterion for the presence of aromatic structure in a molecule (Yassine et al., 2014).

3 Results and discussion

3.1 Organic compounds dominate the growth of new particles initiated by iodine nucleation

Although our offline technique did not allow us to probe nucleating cluster composition at ~ 1.7 nm, four facts from our observation support that the NPF events from 9 to 11 May were initiated by iodine nucleation. First, strong I-NPF events were observed almost every sunny day in April and May, which was the growth and farming season of seaweed. HYSPLIT back-trajectories analysis (Draxler and Rolph, 2010) shows that air masses moved from the East China Sea to the sampling site during the I-NPF days from 8 to 10 May 2018 (Fig. S1b). Sea breeze was also expected to flow from the sea to the site in the daytime when the I-NPF events occurred. Second, the evolution of PNSD from 9 to 11 May was not like banana-shaped C-NPF observed on the winter days but rather was markedly similar to prior reports of iodine nucleation at European coastal sites (Mäkelä et al., 2002; Sipilä et al., 2016). Third, the production of 2–7 nm particles (N_{2-7}) during the C-NPFs followed a nearly identical variation with solar radiation (Fig. S2c), which is an indication that the C-NPFs was initiated by OH and H_2SO_4 production dictated by solar radiation. However, this was not observed during the I-NPF events; instead, N_{2-7} was anticorrelated with tidal height in the daytime (Fig. S2a). Fourth, probably the most important, mean total I in 10–56 nm particles during the I-NPF days (13.5 ng m^{-3}, Table 1) was 67 and 36 times higher than those during the C-NPF days (0.2 ng m^{-3}) and non-event days (0.37 ng m^{-3}), respectively. In the same size range, mean HSO_4^- concentration (0.2 µg m^{-3}) during the I-NPF days was lower than that during the C-NPF days (0.5 µg m^{-3}).

By assuming nanometer-sized particles are spherical with a density of 1.5 g cm^{-3}, we estimate from the PNSD data that aerosol mass in the 10–56 nm size range was enhanced by 3.0 and 1.3 µg m^{-3} at most by the selected I-NPF and C-NPF events (Fig. S2b and d). The fraction of organic mass (OM) in the aerosol mass can be further calculated as $(1.5 \times m_{\mathrm{TOC}})/(m_{\mathrm{Total\ I}} + m^-_{\mathrm{HSO_4}} + 1.5 \times m_{\mathrm{TOC}}) \times 100\,\%$ by assuming an OM/TOC ratio of 1.5. The result shows that mass fractions of OM are 95 %, 87 % and 68 %, respectively, in the size bins 10–18, 18–32 and 32–56 nm during the I-NPF days. Therefore, organic compounds dominate the aerosol mass in the 10–56 nm new particles during the I-NPF days and were critical for I-NPF to contribute to CCN. Our result is qualitatively consistent with previous measurements showing that nucleation mode particles initiated by iodine were composed of a remarkable fraction of organic compounds and sulfate (Mäkelä et al., 2002; Vaattovaara et al., 2006). The main purpose of this article is to identify these organic compounds during the I-NPF days. The OC composition during the C-NPF days is beyond the scope of this article.

3.2 Elemental composition of non-iodinated OC on the I-NPF days

Nontarget analysis of OC elemental composition was performed in detail on 10–18 nm, 32–56 nm, 180–560 nm and 3.2–5.6 µm particles during the I-NPF days. Elemental formulas in the four size bins can represent OC molecular composition of nucleation mode, Aitken mode, accumulation mode and coarse mode, respectively. OC formulas were divided into two categories: non-iodinated OC and iodinated OC. There are far more non-iodinated OC formulas than iodinated OC formulas in < 1 µm particles in terms of both formula number (Table 2) and relative intensity (Fig. 1). For example, 2831 non-iodinated OC formulas account for 96.6 % of OC total intensity in 10–18 nm particles, while 137 iodinated OC formulas account for the remaining 3.4 %. It means that non-iodinated OC dominates new particle growth during the I-NPF events. In this section, we first discuss chemical characteristics of non-iodinated OC, while the speciation of iodinated OC will be discussed in Sect. 3.4.

The molecular formulas of non-iodinated OC were divided into seven elemental groups, CHO^-, CHO^+, $CHON^-$, $CHON^+$, $CHOS^-$, $CHONS^-$ and CHN^+. The number distribution of seven elemental groups for the four size bins is

Table 1. Concentrations of total iodine (I), HSO_4^- and total organic carbon (TOC) in three size bins between 10–56 nm during the I-NPF, C-NPF and non-NPF days. For simplicity, only the sum of three size bins is are shown for the C-NPF and non-NPF days. BDL: below detection limit.

	I-NPF			C-NPF	Non-NPF
	10–18 nm	18–32 nm	32–56 nm	10–56 nm	10–56 nm
Total I ($\mu g\,m^{-3}$)	2.3×10^{-3}	6.2×10^{-3}	5.0×10^{-3}	0.20×10^{-3}	0.37×10^{-3}
HSO_4^- ($\mu g\,m^{-3}$)	2.2×10^{-2}	3.4×10^{-2}	14.4×10^{-2}	50×10^{-2}	BDL
TOC ($\mu g\,m^{-3}$)	3.1×10^{-1}	1.8×10^{-1}	2.1×10^{-1}	2.8×10^{-1}	BDL

Table 2. The numbers of assigned formulas of elemental groups of organic compounds in 10–18 nm, 32–56 nm, 180–560 nm and 3.2–5.6 µm size bins. The first four rows show the percent of formula repeatability between two size bins. 1I-OC: molecular formula containing one iodine atom.

Repeatability	10–18 nm	32–56 nm	180–560 nm	3.2–5.6 µm		
10–18 nm		58 %	25 %	4 %		
32–56 nm	57 %		38 %	4 %		
180–560 nm	34 %	51 %		6 %		
3.2–5.6 µm	35 %	35 %	34 %			
Non-iodinated OC					Total	
CHO^-	531	565	525	20	892	
CHO^+	250	501	380	111	857	
$CHON^-$	1005	638	347	25	1268	
$CHON^+$	1139	1055	828	72	2121	
$CHOS^-$	147	216	256	22	357	
$CHONS^-$	134	131	93	10	259	
CHN^+	34	26	7	7	46	
Total	2831	2770	2151	266	4979	
Iodinated OC					Total	1I-OC (%)
$CHOI^-$	32	53	11	5	80	64 %
$CHOI^+$	17	85	31	31	136	93 %
$CHONI^-$	52	29	7	7	77	88 %
$CHONI^+$	34	57	18	52	132	81 %
$CHOSI^-$	3	8	7	3	18	72 %
$CHONSI^-$	2	7	3	2	13	62 %
$CHNI^+$	6	4	4	3	16	56 %
CHI^-	4	2	1	4	9	67 %
Total	137	228	76	100	440	80 %

listed in Table 2. If both $[M + Na]^+$ and $[M + H]^+$ adducts of a formula were detected, the formula was counted only once. It should be noted that some formulas were repeatedly detected in ESI+ and ESI− modes. Some formulas detected in one size bin were also detected in another size bin. This is quantitatively shown in the first four rows of Table 2. For instance, 58 %, 25 % and 4 % of the formulas detected in 10–18 nm aerosols were also detected in 32–56 nm, 180–560 nm and 3.2–5.6 µm aerosols, respectively. In other words, the particles in neighboring size bins share more similarity in organic composition. An unexpected finding is that the number of non-iodinated OC formulas detected in 3.2–5.6 µm coarse particles ($n = 266$) is 1 order of magnitude lower than those of other bins. Reconstructed mass spectra of the seven elemental groups in ESI− and ESI+ modes are shown in Fig. S3 for the four size bins.

CHON is the most commonly assigned elemental group in both ESI+ (2121 $CHON^+$) and ESI− (1268 $CHON^-$) modes, followed by the CHO group (857 CHO^+ formulas and 892 CHO^- formulas). S-containing formulas are 357 $CHOS^-$ and 259 $CHONS^-$. The formula number of the least common CHN^+ group is only 46. In terms of relative intensity, the CHON fraction in the ESI− mode decreases from 61 % of OC in the 10–18 nm bin to 20 % in the 180–560 nm

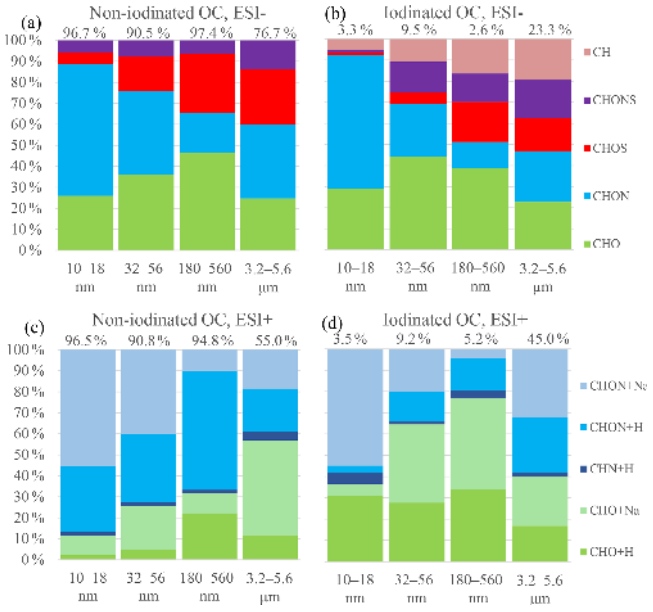

Figure 1. Relative intensity distributions of elemental groups observed in 10–18 nm, 32–56 nm, 180–560 nm and 3.2–5.6 µm size bins in ESI+ and ESI− modes. The percentage above a column denote the percent of non-iodinated OC (or iodinated OC) intensity in total OC intensity in a size bin. +Na and +H denote $[M + \mathrm{Na}]^+$ and $[M + \mathrm{H}]^+$ adduct in ESI+ mode, respectively.

bin (Fig. 1a), while the fractions of CHO and CHOS/CHONS increase with particle size. In the ESI+ mode, the fraction of CHON decreases from 88 % in 10–18 nm bin to 70 % in 180–560 nm bin, being always the dominant elemental group of non-iodinated OC (Fig. 1b). Low-molecular-weight (LMW) amines are important stabilizers in acid–base nucleation (Kurtén et al., 2008; Jen et al., 2014; Zheng et al., 2000; Yao et al., 2016), but their molecular ions are out of the mass range of our FT-ICR-MS. The CHN^+ formulas that we observed contained 9–50 C atoms and 1–7 N atoms, accounting for a negligible fraction, 1.7 %, of total intensity of all ESI+ formulas in the 10–18 nm particles.

Previous elemental composition studies using FT-ICR-MS were mostly conducted on $PM_{2.5}$ or PM_{10} collected from marine (Schmitt-Kopplin et al., 2012; Bao et al., 2018; Ning et al., 2019), urban (Wu et al., 2019; Jiang et al., 2016), free troposphere (Schum et al., 2018; Mazzoleni et al., 2012) and forest sites (Kourtchev et al., 2013). In general, these studies showed that the numbers of CHO compounds were comparable with or more than those of CHON compounds. Our study shows clearly that elemental composition of aerosol OC is highly size dependent. New particle growth in the size range of 10–18 nm during the I-NPF event is dominated by the CHON elemental group, followed by CHO. The focus of this article narrows in on the identity and source of the CHON and CHO formulas in 10–18 nm particles, by comparing with those in the 180–560 nm size bin.

3.2.1 CHO formulas

There is a total of 531 CHO^- formulas and 250 CHO^+ formulas in 10–18 nm particles. There are 54 CHO formulas commonly found in ESI+ and ESI− modes. In terms of relative intensity, CHO^- compounds are more abundant than CHO^+ compounds (Fig. 3b, total intensity: 4.14×10^9 vs. 1.24×10^9). However, this is not indicative of absolute concentration of the two groups due to different ionization efficiency between ESI− and ESI+ modes. CHO^- is characterized by a series of formulas with 20, 24, 28 and 33 C atoms, four or six O atoms, and one equivalent double bond (Fig. 2b). The total intensity of the top 10 formulas accounts for 30 % of all 531 formulas. Assuming CHO^- formulas contain at least one carboxylic group (–COOH), the rest of their molecules should be saturated (DBE = 0) and contain two or four O atoms.

The above feature is not seen in either CHO^+ formulas in the 10–18 nm bin or CHO^- formulas in the 180–560 nm bin. There are more C_{21} and C_{24} formulas than other C subgroups in the CHO^+ formulas of the 10–18 nm bin (Fig. S4d), but none of them have exceptionally high intensity. The prominent formulas in the CHO^- group in 180–560 nm particles have a relatively high unsaturation degree (DBE = 3–7; Fig. 2d). The relative intensities of subgroups according to C atom number in the CHO^- formulas in the 180–560 nm bin are characterized by trimodal distribution with maximum intensity around C_9, C_{13}–C_{16} and C_{20} (Fig. 3d). The relative intensity of O atom subgroups is mono-modally distributed around O_7 (Fig. S5).

3.2.2 CHON formulas

As discussed earlier, CHON is the most abundant elemental group observed in the smallest size bin 10–18 nm. There is a total of 1005 $CHON^-$ formulas (total intensity 9.96×10^9) and 1139 $CHON^+$ formulas (6.45×10^9) in 10–18 nm bin. There are 355 CHON formulas commonly found in ESI+ and ESI− modes. A close examination of Figs. 2a and 3a reveals that $CHON^-$ is characterized by a series of C_{18} and C_{30} formulas with low DBE values (1–4). The 87 C_{18} and 26 C_{30} formulas account for 37 % of total intensity of $CHON^-$. Such a feature is not seen for $CHON^+$ formulas that are rather uniformly distributed in the DBE vs. C diagram (Fig. S4a and c). Generally speaking, $CHON^-$ compounds should contain a nitro- (–NO_2) or nitrooxy- (–ONO_2) group and are ionizable due to the presence of –COOH or hydroxy (–OH) (Lin et al., 2012). However, the presence of an amine group in $CHON^-$ formulas cannot be excluded. Take C_{18} as an example: 51 out of 87 $C_{18}H_hO_oN_n^-$ formulas should contain at least one amine group, either because their O atom numbers are not large enough to allow the assignment of –NO_2 for all N atoms or because some formulas (25 out of 87) were also detected in ESI+ mode. In total, 51 $C_{18}H_hO_oN_n^-$ formulas

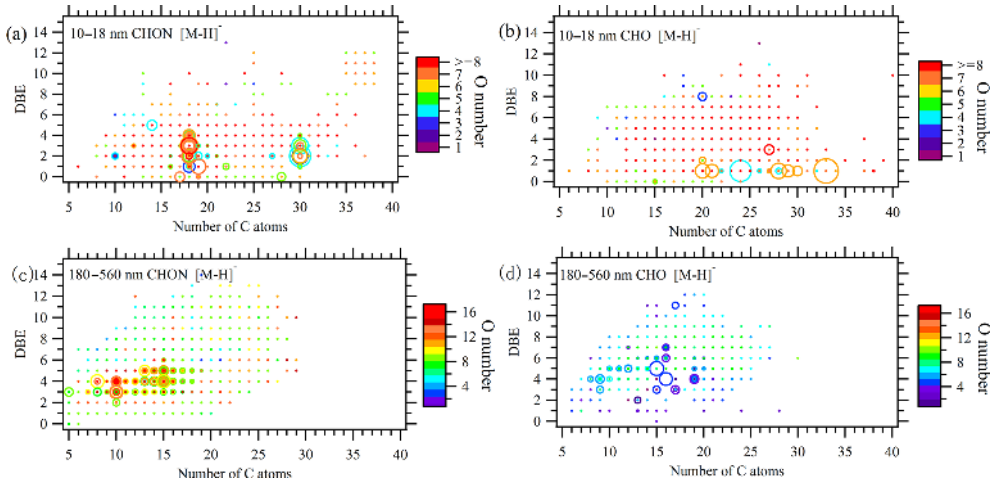

Figure 2. DBE vs. C atom number diagrams of all CHON and CHO formulas detected in 10–18 and 180–560 nm particles in ESI− mode. The color bar denotes O atom number in the formulas. The size of the circles reflects the relative intensities of molecular formulas on a logarithmic scale.

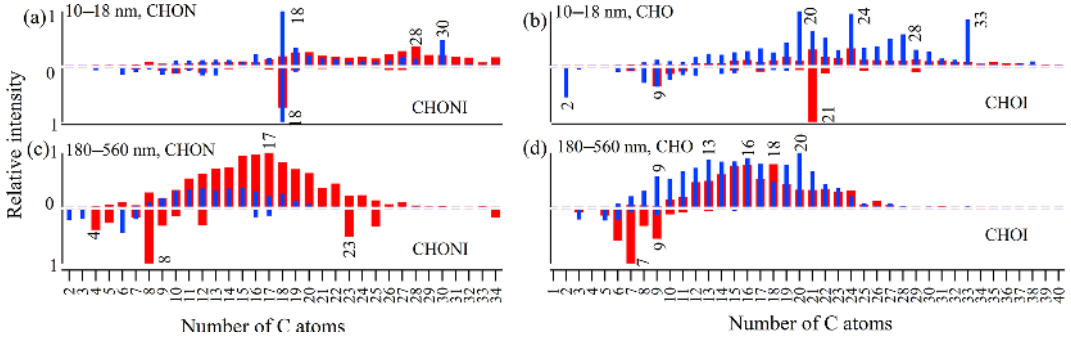

Figure 3. Relative intensities of subgroups according to C atom number in CHON, CHO, CHONI and CHOI formulas in 10–18 and 180–560 nm particles in ESI+ (in red) and ESI− (in blue). The intensity of the most abundant subgroup in a size bin is defined as 1, and those of other subgroups are normalized by it. The relative intensities of non-iodinated OC formulas (iodinated OC formulas) are plotted in the region above (below) the zero line.

with an amine group account for 54.4 % of total intensity of 87 $C_{18}H_hO_oN_n^-$ formulas.

The presence of an amine group in $C_{18}H_hO_oN_n^-$ formulas in 10–18 nm particles is also supported by the comparison with $CHON^-$ in 180–560 nm submicron aerosols. $CHON^-$ in 180–560 nm is characterized by a number of formulas with maximum intensity around C_{10} and C_{15} (Fig. 2c). A plot of O atom number vs. N atom number in Fig. S6a shows that $C_{10}H_hO_oN_n^-$ formulas in 180–560 nm have O/N ratios ≥ 3, and the O atom number is positively correlated with N atom number. It indicates that these $C_{10}H_hO_oN_n^-$ formulas are probably nitro- or nitrooxy- oxidation products of monoterpenes from continental plant emission. In contrast, O/N ratios of the $C_{18}H_hO_oN_n^-$ formulas in 10–18 nm are mostly small, and the O atom number does not increase with N atom number (Fig. S6b). All the collective evidence above reveals that nitrogen-containing organic compounds in 10–18 nm particles during the I-NPF days are partly composed of long-chain amino alcohols, amino acids and so on.

In summary, a series of very distinctive $CHON^-$ and CHO^- formulas was observed in 10–18 nm new particles during the I-NPF days. These formulas are characterized by some specific numbers of C atoms (i.e., $C_{18}H_hO_oN_n$, $C_{30}H_hO_oN_n$, $C_{20}H_hO_o$, $C_{24}H_hO_o$, $C_{28}H_hO_o$ and $C_{33}H_hO_o$) and equivalent double bonds (DBE = 1 for CHO^- and 1–4 for $CHON^-$). The monomer–dimer distribution pattern that can arise from particle-phase oligomerization (Pospisilova et al., 2020) was not observed for these formulas in the mass spectra. We also assume that $C_{18,30}H_hO_oN_n$ and $C_{20,24,28,33}H_hO_o$ are not labile intermediates like ester hydroperoxides that may undergo fast decomposition in the particles or during the sample preparation process (Zhao et al., 2018a, b). To the best of our knowledge, such $CHON^-$ and CHO^- formulas have not been reported by previous aerosol studies. The chemical composition of new parti-

cles is completely decoupled from the CHO^- and $CHON^-$ formulas around C_{10}, C_{15} and C_{20} in 180–560 nm submicron particles, which might be originated from continental terpene emissions. Fewer O atoms in $C_{18,30}H_hO_oN_n$ and $C_{20,24,28,33}H_hO_o$ formulas than those in submicron aerosols indicate that these compounds should be more freshly emitted into the atmosphere. The discontinuous chemical composition and PNSD spectrum (Fig. S2b) below and above 50 nm particle size reflect the fact that the further growth of new particles beyond 50 nm in local I-NPF events cannot be monitored by our stationary sampling strategy.

On the other hand, we observed more complicated distributions of CHO^+ and $CHON^+$ formulas in 10–18 nm new particles that are of relatively small individual intensity and are rather uniformly distributed in DBE vs. C diagrams. Like $CHON^-$ and CHO^-, those CHO^+ and $CHON^+$ formulas also possess a larger number of C atoms ($C > 19$) than their counterparts in 180–560 nm submicron aerosols (Fig. 3). In fact, 21 out of 30 of the most abundant $CHON^+$ formulas contain two or more N atoms; this ratio 21/30 is higher than those in $CHON^-$ formulas. Generally speaking, CHO^+ and $CHON^+$ formulas represent carbonyls / alcohols / epoxides and amino alcohols / amino acids, respectively. One interesting finding about CHO^+ and $CHON^+$ is that they tend to form $[M+Na]^+$ adducts in small aerosols and $[M+H]^+$ adducts in large aerosols (Fig. 1c). This indicates that the CHO^+ and $CHON^+$ compounds in new particles during the I-NPF days should possess different basic functional groups from those in submicron particles.

3.3 Possible precursors and formation mechanism of organic compounds detected in 10–18 nm new particles during the I-NPF days

It is unrealistic to simply propose one out of a large number of possible structures for a formula with large C atom number (e.g., ≥ 18). Our strategy is to first explore the possible precursors of the newly found $C_{18,30}H_hO_oN_n$ and $C_{20,24,28,33}H_hO_o$ formulas. Obviously, $C_{18,30}H_hO_oN_n$ and $C_{20,24,28,33}H_hO_o$ formulas cannot be attributed to continental terpene emission or anthropogenic aromatic emissions. Sporadic spikes of 10–18 nm particles that can be an indication of cooking and traffic emissions were not seen in the PNSD spectrum, because such human activities were rare around the site during the sampling period. We thus also exclude the possibility of cooking and traffic emissions.

Previous field measurements of marine NPF precursor focused on volatile species like iodine (Stevanović et al., 2019), iodomethanes (O'Dowd et al., 2002), dimethyl sulfonic acid (Yvon et al., 1996; Barone et al., 1996; Barnes et al., 2006) and LMW amines (Ning et al., 2019; Ge et al., 2011). So far there is no report about aliphatic compounds with C number ≥ 18 in either gas-phase or new particles (Cochran et al., 2017; Bikkina et al., 2019). Therefore, we consulted the literature that reported chemical compounds isolated from biological tissues of algae, plankton or other marine organisms. Potential precursors are listed in Table 3.

3.3.1 Fatty acids

Fatty acids (FAs) are widely found in animals, plants and microbes (Moss et al., 1995). Plants have a higher content of unsaturated FAs than animals. C_{14}–C_{24} fatty acids, including both saturated and unsaturated, have long been observed in seaweed (Dawczynski et al., 2007). Very long chain FAs (C_{24}–C_{36}) have been isolated from green algae, chlorella kessleri, sponges and marine dinoflagellate (Litchfield et al., 1976; Řezanka and Podojil, 1984; Mansour et al., 1999). C_{18} Oleic acid, linoleic acid and linolenic acid are the most commonly found unsaturated FAs in macro algae. FAs with a carbon chain shorter than C_{20} were used by atmospheric chemists as organic tracers of atmospheric aerosols from microbe or kitchen emission (Simoneit and Mazurek, 1982; Zheng et al., 2000; Guo et al., 2003; Rogge et al., 1991; DeMott et al., 2018; Willoughby et al., 2016). In our study, no saturated FAs were detected in 10–18 nm particles. Only 1.5 % of CHO^- formulas can be assigned to unsaturated FAs (that is, include two O atoms, 14–28 C atoms and DBE = 3–6). Other CHO compounds observed in 10–18 nm particles contain more than two O atoms and thus can be assigned as the oxidized derivatives of FAs.

Possible oxidation schemes of two typical C_{18} ($C_{18}H_{30}O_2$, α-linolenic acid, three C=C double bonds in the carbon chain) and C_{28} unsaturated FAs ($C_{28}H_{52}O_2$, two C=C double bonds), for instance, are proposed in Figs. S7 and S8. The reaction of an unsaturated FA after the emission into the atmosphere is initiated by OH addition to a C=C double bond and subsequent O_2 addition to form a peroxy radical (Atkinson et al., 1995; Calvert et al., 2000). Depending on the level of NO and reactivity, four competitive pathways are available for peroxy radicals to produce CHO or CHON formulas observed in our study: reaction with NO to form a $–ONO_2$ group (pathway 1) or an alkoxy radical that further reacts with O_2 to form a carbonyl (–C=O, pathway 2), reaction with RO_2 radicals to form a hydroxyl (–OH) or a –C=O group (pathway 3), and successive intermolecular H-shift/O_2 addition autoxidation (Crounse et al., 2013; Vereecken et al., 2015) (pathway 4).

Pathways 1 and 2 add $–ONO_2$, –OH and –C=O groups to the carbon chain but do not reduce the DBE of the FA precursor. We propose that pathways 1 and 2 are preferred for those FAs with higher reactivity with NO (e.g., α-linolenic acid; Fig. S7). α-linolenic acid oxidation in the atmosphere via sequential occurrences of pathways 1 or 2 yields a series of oxygenated and nitrated organic compounds, among which $C_{18}H_{31}NO_6$, $C_{18}H_{31}NO_8$, $C_{18}H_{31}NO_{10}$, $C_{18}H_{32}N_2O_{10}$ and $C_{18}H_{33}N_3O_4$ are found in 10–18 nm particles. These formulas explain the circles with DBE = 4 and C number = 18 shown in Fig. 2a (DBE vs. C atom number diagram).

Table 3. Possible precursors and their presence in marine biological sources and our aerosol samples. ND: not detected.

	Potential precursors	Presence in marine sources	Presence in aerosol particles
Unsaturated fatty acid	C_{14}–C_{24} fatty acids	Seaweed (Dawczynski et al., 2007)	1.5 % of CHO^- in terms of relative intensity
	C_{25}–C_{36} very long chain fatty acids	Green algae, chlorella kessleri, sponges, marine dinoflagellate (Litchfield et al., 1976; Řezanka and Podojil, 1984; Mansour et al., 1999).	ND
Fatty alcohols	C_{30}–C_{32} mono- and diunsaturated alcohols and diols	Yellow-green algae (Volkman et al., 1992) (eustigmatophytes)	ND
Saturated hydroxyl fatty acids	$C_{20}H_{40}O_3$, $C_{32}H_{64}O_4$	Nannochloropsis, cutins and suberins of higher plants (Gelin et al., 1997).	S/N 15 and 28
Nonprotein amino acid	$C_{18}H_{37}NO_4$ saturated dihydroxy amino acid (simplifungin,	Marine fungal metabolites (Ishijima et al., 2016; VanMiddlesworth et al., 1992).	S/N 280
	$C_{20–22}H_{39–41}NO_{5–7}$ monounsaturated polyhydroxy amino acids in sphigolipids		S/N 30–230
Amino alcohols	$C_{16–28}H_{33–53}NO_{1–4}$ polyhydroxy amino alcohols	Plant biomembrane, secondary metabolites in marine organisms (Jares-Erijman et al., 1993).	S/N 23–640
	$C_{18}H_{31}NO$ and $C_{18}H_{29}NO$ polyunsaturated amino alcohols	Mediterranean tunicate (Jares-Erijman et al., 1993)	S/N 10–60
	$C_{18}H_{36}N_2O_5$ polyhydroxy cyclic alkaloid	Moraceae (Tsukamoto et al., 2001)	S/N 800

The net outcome of sequential pathway 3 and 4 reactions is to add –OH and –C=O groups and reduce the DBE of the FA precursor. We propose that pathways 3 and 4 are preferred for those FAs (e.g., C_{28} FA $C_{28}H_{52}O_2$) with higher reactivity with RO_2 (Fig. S8). The end products are a series of $C_{28}H_{52}O_{6–8}$, $C_{28}H_{54}O_{4–7}$ and $C_{28}H_{56}O_{6–8}$ compounds, which can explain the circles with C number = 28 and DBE = 1–3 in Fig. 2b.

In addition to fatty acids, fatty alcohols such as C_{30}–C_{32} mono- and diunsaturated alcohols and diols have been detected in yellow-green algae (Volkman et al., 1992). Although these unsaturated alcohols were not detected in our 10–18 nm particles, we suppose that they or their metabolites in algae may undergo similar reactions like unsaturated FA to generate condensable oxygenated and nitrated fatty alcohols in the atmosphere. Hydroxy fatty acids (HFAs) are important constituents of lipid in marine microalgae (Gelin et al., 1997), bacteria (Kim and Oh, 2013), seaweed (Kendel et al., 2013; Blokker et al., 1998) and leaf surface of higher plants (Pollard et al., 2008). Among them, two saturated HFAs, $C_{20}H_{40}O_3$ and $C_{32}H_{64}O_4$, were found in our 10–18 nm aerosol sample with S/N ratios 15 and 28. However, because saturated hydroxy fatty acids are not oxidizable via the pathways proposed in our study, they are assumed unlikely to be precursors of other formulas observed in 10–18 nm particles.

3.3.2 Nonprotein amino acids and amino alcohols

Quantum chemical calculations have showed that amino acids like glycine, serine and threonine are potential participants in atmospheric nucleation via interaction with sulfuric acid (Elm et al., 2013; Ge et al., 2018; Li et al., 2020). However, we did not observe any of 20 essential amino acids in 10–18 nm in either ESI+ or ESI− modes. One reason may be that most essential amino acids have molecular weight less than 150, which is below mass scan range of our FT-ICR-MS.

There are a number of records in the literature about long-chain nonprotein amino acids or amino alcohols isolated from marine organisms or plant biomembrane (Ishijima et al., 2016; VanMiddlesworth et al., 1992; Jares-Erijman et al., 1993; Tsukamoto et al., 2001). They include saturated dihydroxy amino acid ($C_{18}H_{37}NO_4$, DBE = 1, simplifungin), monounsaturated polyhydroxy amino acids in sphigolipids ($C_{20–22}H_{39–41}NO_{5–7}$, DBE = 2–3), polyhydroxy amino alcohols ($C_{16–28}H_{33–53}N_{1–2}O_{1–5}$, DBE = 1–3, sphingosine and its natural metabolites) and polyunsaturated amino alcohols ($C_{18}H_{31}NO$ and $C_{18}H_{29}NO$, DBE = 4–5). All of these for-

mulas were detected in 10–18 nm aerosols with S/N in the range of 10–800. More importantly, all those compounds that contain at least one amine group and one C=C double bond can be precursors of observed CHON formulas containing an amine group via the pathways that we showed above. As an example, the oxidation scheme of an amino alcohol $C_{18}H_{31}NO$ with 4 C=C double bonds in the carbon chain is illustrated in Fig. S9.

Similar to C_{28} FA, $C_{18}H_{31}NO$ undergoes successive intermolecular H-shift/O_2 additions to produce a series of RO_2 radicals with a hydroperoxyl group (–OOH) in its carbon chain. The subsequent pathway 3 reactions, as well as the decomposition of –OOH groups, add –OH and –C=O groups in the carbon chain. Because $C_{18}H_{31}NO$ possesses as many as four C=C double bonds, sequential pathways 3 and 4 reactions produce a large number of oxidation products, among which 57 are found in the formula list detected in 10–18 nm particles (Fig. S9). These products $C_{18}H_{31}NO_{4-11,13}$, $C_{18}H_{33}NO_{4,6-10}$, $C_{18}H_{35}NO_{5-9}$, $C_{18}H_{37}NO_{7-12}$ and $C_{18}H_{39}NO_{10\text{-}11}$ explain perfectly the presence of a series of formulas with C number = 18, DBE = 0–4 and a $–NH_2$ group shown in Fig. 2a.

3.3.3 Volatility estimation

Based on the reaction mechanisms proposed above, it is possible to estimate the volatility change from potential precursors to their oxidation products. First, from the list of elemental formulas detected in 10–18 nm particles, we select 49 formulas with high intensities, including 14 $CHON^-$ formulas with peak intensity $> 1.00 \times 10^8$, 23 $CHON^+$ formulas with peak intensity $> 3.00 \times 10^7$ and 12 CHO^- formulas (DBE = 1) with peak intensities $> 3.00 \times 10^7$. Possible combinations of –COOH, $–ONO_2$, –C=O, C=C double bond, $–NH_2$ and –OH groups are searched for every formula obeying two simple rules: $CHON^-$ and CHO^- formulas must possess a carboxyl or hydroxyl group; $CHON^+$ formulas must possess an amino group. Saturation concentration (C^*) values of the 49 formulas were then predicted for all combinations using a simple group contribution method developed by Pankow and Asher (2008). On the other hand, the C^* of their possible precursors, including unsaturated FAs, fatty alcohols, nonprotein amino acids or amino alcohols, were predicted by the same method.

As we can see in Table S4 in the Supplement, C^* values of the 49 formulas fall into the range of ELVOCs (extremely low volatility organic compounds; 3×10^{-9}–3×10^{-5} $\mu g\,m^{-3}$) and even ULVOCs (ultra low volatility organic compounds; $< 3 \times 10^{-9}$ $\mu g\,m^{-3}$), while C^* values of their precursors are in the range of SVOCs (semivolatile organic compounds; 0.3–300 $\mu g\,m^{-3}$) or LVOCs (3×10^{-5}–0.3 $\mu g\,m^{-3}$). The addition of functional groups reduces the volatility of precursors by 2–7 orders of magnitude and thus makes their oxidation products condensable onto new particles during the I-NPF event days. According to the definition of Schervish and Donahue (2020) and Simon et al. (2020), ULVOCs can even drive pure biogenic nucleation. Therefore, the analysis of precursor-product volatility partly supports our hypothesis about the molecular identity and formation mechanism of the formulas detected in 10–18 nm particles. It should be noted that the volatility of VOC oxidation products can be assessed with numerous existing parameterizations, which require either exact functional groups or only the molecular formula (Peräkylä et al., 2019). Their estimation can vary by up to several orders of magnitude. But this will not change the conclusion drawn here.

3.4 Speciation of iodinated OC

Organic iodine compounds hold the key to understanding aerosol iodine chemistry and its role in regulating the recycling of halogens to the gas phase. We identified 440 iodinated OC formulas from the four size bins during the I-NPF days (Table 2). Eighty percent of the 440 formulas contain one I atom, and the rest of them contain two I atoms. In terms of relative intensity, iodinated OC accounts for 2.6 %–9.5 % of OC in fine particles, but its fraction in coarse particles increases to 23.3 % in ESI− mode and 45 % in ESI+ mode. The size distribution of seven iodinated OC groups (i.e., $CHOI^-$, $CHONI^-$, $CHOSI^-$, $CHONSI^-$, $CHOI^+$, $CHONI^+$ and $CHNI^+$) resembles those of non-iodinated OC groups (Fig. 1). If we replace I atom(s) with H atom(s) in a formula, 107 out of 440 replaced formulas are also found in the non-iodine OC formula list.

Iodinated OC with intensity $> 1.00 \times 10^7$ in the four size bins were shown in Fig. 4. The DBE vs. C diagram for 10–18 nm particles is characterized by (1) nine $C_{18}H_hO_oN_nI$ formulas with DBE = 1–4 and (2) $C_9H_{16}NO_3I$ and its C_{10}–C_{13} homologues. Because these formulas were detected in ESI+ mode, they are most likely iodinated amino acids. The 32–56 nm particles accommodate the most abundant iodinated OC formulas, in terms of both formula number and relative intensity. Prominent formulas include (1) diiodo acetic acid $C_2H_2O_2I_2$, diiodomethane CH_2I_2, (2) iodinated C_{21} carbonyls $C_{21}H_{39}OI$ and $C_{21}H_{41}OI$, (3) iodinated $C_{21,25,27,29}$ alcohols or ethers with DBE = 0, (4) iodinated C_{10} and C_{15} terpene and sesquiterpene oxidation products, and (5) iodinated organic sulfate $C_8H_{17}N_2SO_8I$ and $C_{21}H_{43}SO_4I$. In addition, $C_9H_{10}NO_3I$ detected in this size bin (S/N ratio: 35) can be tentatively assigned to an iodinated amino acid iodotyrosine that has been observed in seaweed (Yang et al., 2016), implying direct contribution from seaweed emission to new particles.

In 180–560 nm particles, the majority of iodinated OC are C_{6-9} aromatic $CHOI^+$ compounds with AI > 0.5 and DBE = 5–7. Both C and O atom numbers of these iodinated OC are smaller than those of mono-modally distributed CHO^+ compounds around C_{15} in the same particle size (Figs. 3d and S3b). This implies that iodine has a strong tendency to aromatic compounds in submicron aerosols due

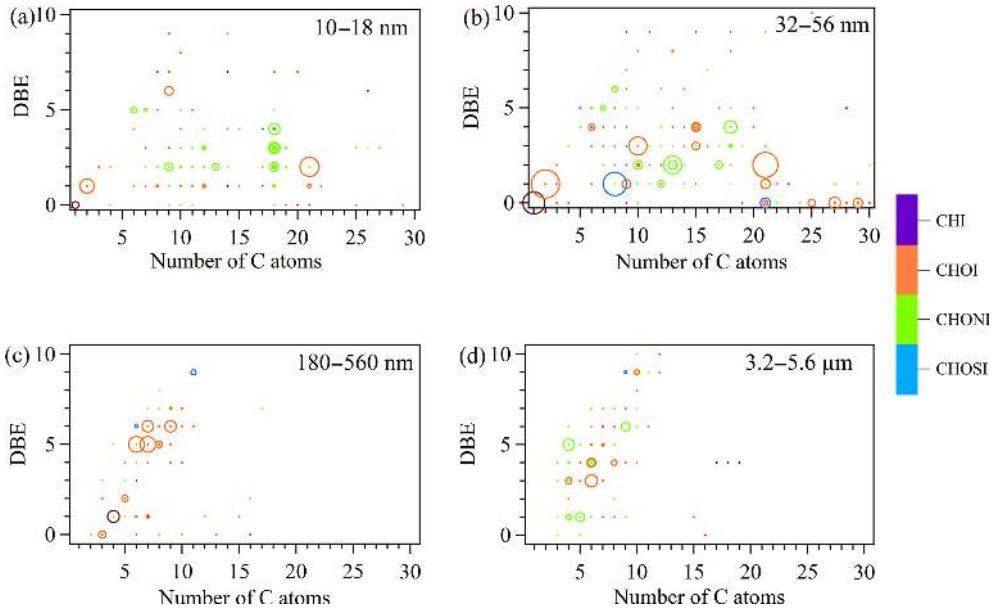

Figure 4. DBE vs. C atom number diagrams of iodinated OC formulas with intensity $> 1.00 \times 10^7$ in the four size bins. The color bar denotes the elemental groups of assigned formulas. The size of the circles reflects the relative intensities of molecular formulas on a logarithmic scale.

to electrophilic substitution on aromatic rings. In 3.2–5.6 µm particles, iodinated OC features C_4–C_6 CHO^+ and $CHON^+$ compounds with DBE = 3–6, which again have fewer C atoms than non-iodinated OC. Supporting evidence from AI shows these compounds are not aromatic. Coastal 3.2–5.6 µm particles can be sea salt particles formed during bubble bursting of seawater (Russell et al., 2010; Schmitt-Kopplin et al., 2012; Quinn et al., 2014; Wilson et al., 2015). However, Hao et al. (2017) showed that iodinated OC products from the reaction between iodine and seawater are highly unsaturated carboxylic-rich polyphenols with DBE = 4–14 and C atoms = 10–30. It is thus apparent that iodinated OC in 3.2–5.6 µm particles was not directly from iodinated organic compounds in the seawater.

3.5 Atmospheric implications

Due to the 71 % ocean coverage of the Earth's surface, marine aerosol generation is important in determining the Earth's radiative budget and climate change. Of the limited number of studies reporting coastal NPF, most have focused on iodine emission, oxidation and nucleation in the early stage of NPF. In principle, abundant low-volatility condensing vapors other than iodine are required in coastal environments for the growth of iodine clusters to CCN. This article reveals a new group of important organic compounds involved in this process. It is most likely that their precursors are emitted mutually with iodine from direct exposure of coastal biota to either the atmosphere or biologically active sea surface. If this is true, we suggest the results in our location can be extrapolated to other iodine-rich coastal locations, as long as iodine-NPF can be observed. More fundamental field, laboratory and modeling studies are needed to determine (1) exact emission sources and source rates of these organic precursors, (2) their gas-phase intermediates and oxidation mechanisms in the atmosphere, and (3) their quantitative contribution to global and regional CCN numbers.

Data availability. All of the datasets related to the chemical formulas detected in this work can be accessed via https://doi.org/10.3974/geodb.2020.03.26.V1 (Yu, 2020). Any other data used in this publication are available from the corresponding author Huan Yu (yuhuan@cug.edu.cn) upon request.

Supplement. The supplement related to this article is available online at: https://doi.org/10.5194/acp-20-9821-2020-supplement.

Author contributions. HY designed and conducted chemical analysis. YW and HY did data analysis and wrote the paper. XH conducted the field sampling. BJ and YL did the FT-ICR-MS analysis. BK, ML, DX, JC and JZY reviewed and revised the paper.

Competing interests. The authors declare that they have no conflict of interest.

Special issue statement. This article is part of the special issue "Marine organic matter: from biological production in the ocean to

organic aerosol particles and marine clouds (ACP/OS inter-journal SI)". It is not associated with a conference.

Financial support. This research has been supported by the National Science Foundation of China (grant nos. 41975831 and 41675124) and the National Key Research and Development Program of China (grant no. 2016YFC0203100).

Review statement. This paper was edited by Manuela van Pinxteren and reviewed by two anonymous referees.

References

Allan, J. D., Williams, P. I., Najera, J., Whitehead, J. D., Flynn, M. J., Taylor, J. W., Liu, D., Darbyshire, E., Carpenter, L. J., Chance, R., Andrews, S. J., Hackenberg, S. C., and McFiggans, G.: Iodine observed in new particle formation events in the Arctic atmosphere during ACCACIA, Atmos. Chem. Phys., 15, 5599–5609, https://doi.org/10.5194/acp-15-5599-2015, 2015.

An, Y., Xu, J., Feng, L., Zhang, X., Liu, Y., Kang, S., Jiang, B., and Liao, Y.: Molecular characterization of organic aerosol in the Himalayas: insight from ultra-high-resolution mass spectrometry, Atmos. Chem. Phys., 19, 1115–1128, https://doi.org/10.5194/acp-19-1115-2019, 2019.

Atkinson, R., Tuazon, E. C., and Aschmann, S. M.: Products of the Gas-Phase Reactions of a Series of 1-Alkenes and 1-Methylcyclohexene with the OH Radical in the Presence of NO, Environ. Sci. Technol., 29, 1674–1680, https://doi.org/10.1021/es00006a035, 1995.

Bao, H. Y., Niggemann, J., Li, L., Dittmar, T., and Kao, S.-J.: Molecular composition and origin of water-soluble organic matter in marine aerosols in the Pacific off China, Atmos. Environ., 191, 27–35, https://doi.org/10.1016/j.atmosenv.2018.07.059, 2018.

Barnes, I., Hjorth, J., and Mihalopoulos, N.: Dimethyl Sulfide and Dimethyl Sulfoxide and Their Oxidation in the Atmosphere, Chem. Rev., 106, 940–975, https://doi.org/10.1021/cr020529+, 2006.

Barone, S. B., Turnipseed, A. A., and Ravishankara, A. R.: Reaction of OH with Dimethyl Sulfide (DMS). 1. Equilibrium Constant for $OH + DMS$ Reaction and the Kinetics of the $OH^{\bullet}$ $DMS + O_2$ Reaction, J. Phys. Chem. A, 100, 14694–14702, https://doi.org/10.1021/jp960866k, 1996.

Bianco, A., Deguillaume, L., Vaïtilingom, M., Nicol, E., Baray, J.-L., Chaumerliac, N., and Bridoux, M.: Molecular Characterization of Cloud Water Samples Collected at the Puy de Dôme (France) by Fourier Transform Ion Cyclotron Resonance Mass Spectrometry, Environ. Sci. Technol., 52, 10275–10285, https://doi.org/10.1021/acs.est.8b01964, 2018.

Bikkina, P., Kawamura, K., Bikkina, S., Kunwar, B., Tanaka, K., and Suzuki, K.: Hydroxy Fatty Acids in Remote Marine Aerosols over the Pacific Ocean: Impact of Biological Activity and Wind Speed, ACS Earth. Space. Chem., 3, 366–379, https://doi.org/10.1021/acsearthspacechem.8b00161, 2019.

Blokker, P., Schouten, S., van den Ende, H., De Leeuw, J. W., and Sinninghe Damsté, J. S.: Cell wall-specific ω-hydroxy fatty acids in some freshwater green microalgae, Phytochemistry, 49, 691–695, https://doi.org/10.1016/S0031-9422(98)00229-5, 1998.

Burkholder, J. B., Curtius, J., Ravishankara, A. R., and Lovejoy, E. R.: Laboratory studies of the homogeneous nucleation of iodine oxides, Atmos. Chem. Phys., 4, 19–34, https://doi.org/10.5194/acp-4-19-2004, 2004.

Calvert, J. G., Atkinson, R. G., Orlando, J. J., Wallington, T. J., and Tyndall, G. S.: The Mechanisms of Atmospheric Oxidation of Alkenes, Oxford Univ. Press, Oxford, UK, 2000.

Cochran, R. E., Laskina, O., Trueblood, J. V., Estillore, A. D., Morris, H. S., Jayarathne, T., Sultana, C. M., Lee, C., Lin, P., Laskin, J., Laskin, A., Dowling, J. A., Qin, Z., Cappa, C. D., Bertram, T. H., Tivanski, A. V., Stone, E. A., Prather, K. A., and Grassian, V. H.: Molecular Diversity of Sea Spray Aerosol Particles: Impact of Ocean Biology on Particle Composition and Hygroscopicity, Chem. Pharm. Bull, 2, 655–667, https://doi.org/10.1016/j.chempr.2017.03.007, 2017.

Crounse, J. D., Nielsen, L. B., Jørgensen, S., Kjaergaard, H. G., and Wennberg, P. O.: Autoxidation of Organic Compounds in the Atmosphere, J. Phys. Chem. Lett., 4, 3513–3520, https://doi.org/10.1021/jz4019207, 2013.

Daellenbach, K. R., Kourtchev, I., Vogel, A. L., Bruns, E. A., Jiang, J., Petäjä, T., Jaffrezo, J.-L., Aksoyoglu, S., Kalberer, M., Baltensperger, U., El Haddad, I., and Prévôt, A. S. H.: Impact of anthropogenic and biogenic sources on the seasonal variation in the molecular composition of urban organic aerosols: a field and laboratory study using ultra-high-resolution mass spectrometry, Atmos. Chem. Phys., 19, 5973–5991, https://doi.org/10.5194/acp-19-5973-2019, 2019.

Dall'Osto, M., Simo, R., Harrison, R. M., Beddows, D. C. S., Saiz-Lopez, A., Lange, R., Skov, H., Nøjgaard, J. K., Nielsen, I. E., and Massling, A.: Abiotic and biotic sources influencing spring new particle formation in North East Greenland, Atmos. Environ., 190, 126–134, https://doi.org/10.1016/j.atmosenv.2018.07.019, 2018.

Dawczynski, C., Schubert, R., and Jahreis, G.: Amino acids, fatty acids, and dietary fibre in edible seaweed products, Food. Chem., 103, 891–899, https://doi.org/10.1016/j.foodchem.2006.09.041, 2007.

DeMott, P. J., Mason, R. H., McCluskey, C. S., Hill, T. C. J., Perkins, R. J., Desyaterik, Y., Bertram, A. K., Trueblood, J. V., Grassian, V. H., Qiu, Y., Molinero, V., Tobo, Y., Sultana, C. M., Lee, C., and Prather, K. A.: Ice nucleation by particles containing long-chain fatty acids of relevance to freezing by sea spray aerosols, Environ. Sci-Proc. Imp., 20, 1559–1569, https://doi.org/10.1039/c8em00386f, 2018.

Draxler, R. and Rolph, G.: HYSPLIT (HYbrid Single-Particle Lagrangian Integrated Trajectory) model access via NOAA ARL READY website, NOAA Air Resources Laboratory, Silver Spring, MD, available at: http://ready.arl.noaa.gov/HYSPLIT.php (last access: 30 March 2020), 2010.

Ehn, M., Thornton, J. A., Kleist, E., Sipila, M., Junninen, H., Pullinen, I., Springer, M., Rubach, F., Tillmann, R., Lee, B., Lopez-Hilfiker, F., Andres, S., Acir, I. H., Rissanen, M., Jokinen, T., Schobesberger, S., Kangasluoma, J., Kontkanen, J., Nieminen, T., Kurten, T., Nielsen, L. B., Jorgensen, S., Kjaergaard, H. G., Canagaratna, M., Maso, M. D., Berndt, T., Petaja, T., Wahner, A., Kerminen, V. M., Kulmala, M., Worsnop, D. R., Wildt, J., and Mentel, T. F.: A large source of low-

volatility secondary organic aerosol, Nature, 506, 476–479, https://doi.org/10.1038/nature13032, 2014.

Elm, J., Fard, M., Bilde, M., and Mikkelsen, K. V.: Interaction of Glycine with Common Atmospheric Nucleation Precursors, J. Phys. Chem. A, 117, 12990–12997, https://doi.org/10.1021/jp408962c, 2013.

Ge, P., Luo, G., Luo, Y., Huang, W., Xie, H. B., Chen, J. W., and Qu, J. P.: Molecular understanding of the interaction of amino acids with sulfuric acid in the presence of water and the atmospheric implication, Chemosphere, 210, 215–223, https://doi.org/10.1016/j.chemosphere.2018.07.014, 2018.

Ge, X. L., Wexler, A. S., and Clegg, S. L.: Atmospheric amines – Part I. A review, Atmos. Environ., 45, 524–546, https://doi.org/10.1016/j.atmosenv.2010.10.012, 2011.

Gelin, F., Volkman, J. K., De Leeuw, J. W., and Sinninghe Damsté, J. S.: Mid-chain hydroxy long-chain fatty acids in microalgae from the genus Nannochloropsis, Phytochemistry, 45, 641–646, https://doi.org/10.1016/S0031-9422(97)00068-X, 1997.

Guo, Z. G., Sheng, L. F., Feng, J. L., and Fang, M.: Seasonal variation of solvent extractable organic compounds in the aerosols in Qingdao, China, Atmos. Environ., 37, 1825–1834, https://doi.org/10.1016/S1352-2310(03)00064-5, 2003.

Hao, Z. N., Yin, Y. G., Cao, D., and Liu, J. F.: Probing and Comparing the Photobromination and Photoiodination of Dissolved Organic Matter by Using Ultra-High-Resolution Mass Spectrometry, Environ. Sci. Technol., 51, 5464–5472, https://doi.org/10.1021/acs.est.6b03887, 2017.

Ishijima, H., Uchida, R., Ohtawa, M., Kondo, A., Nagai, K., Shima, K., Nonaka, K., Masuma, R., Iwamoto, S., Onodera, H., Nagamitsu, T., and Tomoda, H.: Simplifungin and Valsafungins, Antifungal Antibiotics of Fungal Origin, J. Org. Chem., 81, 7373–7383, https://doi.org/10.1021/acs.joc.6b00952, 2016.

Jares-Erijman, E. A., Bapat, C. P., Lithgow-Bertelloni, A., Rinehart, K. L., and Sakai, R.: Crucigasterins, new polyunsaturated amino alcohols from the mediterranean tunicate Pseudodistoma crucigaster, J. Org. Chem., 58, 5732–5737, https://doi.org/10.1021/jo00073a036, 1993.

Jen, C. N., McMurry, P. H., and Hanson, D. R.: Stabilization of Sulfuric Acid Dimers by Ammonia, Methylamine, Dimethylamine, and Trimethylamine, J. Geophys. Res-Atmos., 119, 7502–7514, https://doi.org/10.1002/2014JD021592, 2014.

Jiang, B., Kuang, B. Y., Liang, Y. M., Zhang, J. Y., Huang, X. H. H., Xu, C. M., Yu, J., and Shi, Q.: Molecular composition of urban organic aerosols on clear and hazy days in Beijing: A comparative study using FT-ICR MS, Environ. Chem., 13, 888–901, https://doi.org/10.1071/EN15230, 2016.

Kendel, M., Barnathan, G., Fleurence, J., Rabesaotra, V., and Wielgosz-Collin, G.: Non-methylene Interrupted and Hydroxy Fatty Acids in Polar Lipids of the Alga Grateloupia turuturu Over the Four Seasons, Lipids, 48, 535–545, https://doi.org/10.1007/s11745-013-3783-5, 2013.

Kim, K. R. and Oh, D. K.: Production of hydroxy fatty acids by microbial fatty acid-hydroxylation enzymes, Biotechnol. Adv., 31, 1473–1485, https://doi.org/10.1016/j.biotechadv.2013.07.004, 2013.

Kourtchev, I., Fuller, S., Aalto, J., Ruuskanen, T. M., McLeod, M. W., Maenhaut, W., Jones, R., Kulmala, M., and Kalberer, M.: Molecular composition of boreal forest aerosol from Hyytiala, Finland, using ultrahigh resolution mass spectrometry, Environ. Sci. Technol., 47, 4069–4079, https://doi.org/10.1021/es3051636, 2013.

Kumar, M., Saiz-Lopez, A., and Francisco, J. S.: Single-Molecule Catalysis Revealed: Elucidating the Mechanistic Framework for the Formation and Growth of Atmospheric Iodine Oxide Aerosols in Gas-Phase and Aqueous Surface Environments, J. Am. Chem. Soc., 140, 14704–14716, https://doi.org/10.1021/jacs.8b07441, 2018.

Kurtén, T., Loukonen, V., Vehkamäki, H., and Kulmala, M.: Amines are likely to enhance neutral and ion-induced sulfuric acid-water nucleation in the atmosphere more effectively than ammonia, Atmos. Chem. Phys., 8, 4095–4103, https://doi.org/10.5194/acp-8-4095-2008, 2008.

Li, D. F., Chen, D. P., Liu, F. Y., and Wang, W. L.: Role of glycine on sulfuric acid-ammonia clusters formation: Transporter or participator, J. Environ. Sci., 89, 125–135, https://doi.org/10.1016/j.jes.2019.10.009, 2020.

Lin, P., Rincon, A. G., Kalberer, M., and Yu, J. Z.: Elemental Composition of HULIS in the Pearl River Delta Region, China: Results Inferred from Positive and Negative Electrospray High Resolution Mass Spectrometric Data, Environ. Sci. Technol., 46, 7454–7462, https://doi.org/10.1021/es300285d, 2012.

Litchfield, C., Greenberg, A. J., Noto, G., and Morales, R. W.: Unusually high levels of C_{24}–C_{30} fatty acids in sponges of the class demospongiae, Lipids, 11, 567–570, https://doi.org/10.1007/BF02532903, 1976.

Mahajan, A. S., Plane, J. M. C., Oetjen, H., Mendes, L., Saunders, R. W., Saiz-Lopez, A., Jones, C. E., Carpenter, L. J., and McFiggans, G. B.: Measurement and modelling of tropospheric reactive halogen species over the tropical Atlantic Ocean, Atmos. Chem. Phys., 10, 4611–4624, https://doi.org/10.5194/acp-10-4611-2010, 2010.

Mahajan, A. S., Gómez Martín, J. C., Hay, T. D., Royer, S.-J., Yvon-Lewis, S., Liu, Y., Hu, L., Prados-Roman, C., Ordóñez, C., Plane, J. M. C., and Saiz-Lopez, A.: Latitudinal distribution of reactive iodine in the Eastern Pacific and its link to open ocean sources, Atmos. Chem. Phys., 12, 11609–11617, https://doi.org/10.5194/acp-12-11609-2012, 2012.

Mäkelä, J. M., Hoffmann, T., Holzke, C., Väkevä, M., Suni, T., Mattila, T., Aalto, P. P., Tapper, U., Kauppinen, E. I., and O'Dowd, C. D., Biogenic iodine emissions and identification of end-products in coastal ultrafine particles during nucleation bursts, J. Geophys. Res., 107, 8110, https://doi.org/10.1029/2001JD000580, 2002.

Mansour, M. P., Volkman, J. K., Holdsworth, D. G., Jackson, A. E., and Blackburn, S. I.: Very-long-chain (C28) highly unsaturated fatty acids in marine dinoflagellates, Phytochemistry, 50, 541–548, https://doi.org/10.1016/S0031-9422(98)00564-0, 1999.

Mazzoleni, L. R., Saranjampour, P., Dalbec, M. M., Samburova, V., Hallar, G. A., Zielinska, B., Lowenthal, D. H., and Kohl, S.: Identification of water-soluble organic carbon in non-urban aerosols using ultrahigh-resolution FT-ICR mass spectrometry: Organic anions, Environ. Chem., 9, 285–297, https://doi.org/10.1071/EN11167, 2012.

Mentel, T. F., Springer, M., Ehn, M., Kleist, E., Pullinen, I., Kurtén, T., Rissanen, M., Wahner, A., and Wildt, J.: Formation of highly oxidized multifunctional compounds: autoxidation of peroxy radicals formed in the ozonolysis of alkenes – deduced from structure–product relationships, Atmos. Chem. Phys., 15, 6745–6765, https://doi.org/10.5194/acp-15-6745-2015, 2015.

Merikanto, J., Spracklen, D. V., Mann, G. W., Pickering, S. J., and Carslaw, K. S.: Impact of nucleation on global CCN, Atmos. Chem. Phys., 9, 8601–8616, https://doi.org/10.5194/acp-9-8601-2009, 2009.

Metzger, A., Verheggen, B., Dommen, J., Duplissy, J., Prevot, A. S. H., Weingartner, E., Riipinen, I., Kulmala, M., Spracklen, D. V., Carslaw, K. S., and Baltensperger, U.: Evidence for the role of organics in aerosol particle formation under atmospheric conditions, P. Natl. Acad. Sci. USA, 107, 6646–6651, https://doi.org/10.1073/pnas.0911330107, 2010.

Moss, G. P., Smith, P. A. S., and Tavernier, D.: Glossary of class names of organic compounds and reactivity intermediates based on structure (IUPAC Recommendations 1995), Pure Appl. Chem., 67, 1307–1375, https://doi.org/10.1351/pac199567081307, 1995.

Ning, C. P., Gao, Y., Zhang, H. J., Yu, H. R., Wang, L., Geng, N. B., Cao, R., and Chen, J. P.: Molecular characterization of dissolved organic matters in winter atmospheric fine particulate matters ($PM_{2.5}$) from a coastal city of northeast China, Sci. Total. Environ., 689, 312–321, https://doi.org/10.1016/j.scitotenv.2019.06.418, 2019.

O'Dowd, C. D., Jimenez, J. L., Bahreini, R., Flagan, R. C., Seinfeld, J. H., Hämeri, K., Pirjola, L., Kulmala, M., Jennings, S. G., and Hoffmann, T.: Marine aerosol formation from biogenic iodine emissions, Nature, 417, 632–636, https://doi.org/10.1038/nature00775, 2002.

Pankow, J. F. and Asher, W. E.: SIMPOL.1: a simple group contribution method for predicting vapor pressures and enthalpies of vaporization of multifunctional organic compounds, Atmos. Chem. Phys., 8, 2773–2796, https://doi.org/10.5194/acp-8-2773-2008, 2008.

Peräkylä, O., Riva, M., Heikkinen, L., Quéléver, L., Roldin, P., and Ehn, M.: Experimental investigation into the volatilities of highly oxygenated organic molecules (HOMs) , Atmos. Chem. Phys., 20, 649–669, https://doi.org/10.5194/acp-20-649-2020, 2020.

Pollard, M., Beisson, F., Li, Y., and Ohlrogge, J. B.: Building lipid barriers: biosynthesis of cutin and suberin, Trends. Plant. Sci., 13, 236–246, https://doi.org/10.1016/j.tplants.2008.03.003, 2008.

Pospisilova, V., Lopez-Hilfiker, F. D., Bell, D. M., El Haddad, I., Mohr, C., Huang, W., Heikkinen, L., Xiao, M., Dommen, J., Prevot, A. S. H., Baltensperger, U., and Slowik, J. G.: On the fate of oxygenated organic molecules in atmospheric aerosol particles, Sci. Adv., 6, 1–12, https://doi.org/10.1126/sciadv.aax8922, 2020.

Pratt, K. A. and Prather, K. A.: Mass spectrometry of atmospheric aerosols–recent developments and applications. Part I: Off-line mass spectrometry techniques, Mass. Spectrom. Rev., 31, 1–16, https://doi.org/10.1002/mas.20322, 2012.

Quinn, P. K., Bates, T. S., Schulz, K. S., Coffman, D. J., Frossard, A. A., Russell, L. M., Keene, W. C., and Kieber, D. J.: Contribution of sea surface carbon pool to organic matter enrichment in sea spray aerosol, Nat. Geosci., 7, 228–232, https://doi.org/10.1038/ngeo2092, 2014.

Řezanka, T. and Podojil, M.: The very long chain fatty acids of the green alga, Chlorella kessleri, Lipids, 19, 472, https://doi.org/10.1007/BF02537412, 1984.

Richters, S., Herrmann, H., and Berndt, T.: Highly Oxidized RO_2 Radicals and Consecutive Products from the Ozonolysis of Three Sesquiterpenes, Environ. Sci. Technol., 50, 2354–2362, https://doi.org/10.1021/acs.est.5b05321, 2016.

Rogge, W. F., Hildemann, L. M., Mazurek, M. A., Cass, G. R., and Simoneit, B. R. T.: Sources of fine organic aerosol. 1. Charbroilers and meat cooking operations, Environ. Sci. Technol., 25, 1112–1125, https://doi.org/10.1021/es00018a015, 1991.

Roscoe, H. K., Jones, A. E., Brough, N., Weller, R., Saiz-Lopez, A., Mahajan, A. S., Schoenhardt, A., Burrows, J. P., and Fleming, Z. L.: Particles and iodine compounds in coastal Antarctica, J. Geophys. Res.-Atmos., 120, 7144–7156, https://doi.org/10.1002/2015JD023301, 2015.

Russell, L. M., Hawkins, L. N., Frossard, A. A., Quinn, P. K., and Bates, T. S.: Carbohydrate-like composition of submicron atmospheric particles and their production from ocean bubble bursting, P. Natl. Acad. Sci. USA, 107, 6652, https://doi.org/10.1073/pnas.0908905107, 2010.

Saiz-Lopez, A. and Plane, J. M. C.: Novel iodine chemistry in the marine boundary layer, Geophys. Res. Lett., 31, L04112, https://doi.org/10.1029/2003GL019215, 2004.

Saiz-Lopez, A., Plane, J. M. C., Baker, A. R., Carpenter, L. J., von Glasow, R., Gómez Martín, J. C., McFiggans, G., and Saunders, R. W.: Atmospheric Chemistry of Iodine, Chem. Rev., 112, 1773–1804, https://doi.org/10.1021/cr200029u, 2012.

Schervish, M. and Donahue, N. M.: Peroxy radical chemistry and the volatility basis set, Atmos. Chem. Phys., 20, 1183–1199, https://doi.org/10.5194/acp-20-1183-2020, 2020.

Schmitt-Kopplin, P., Liger-Belair, G., Koch, B. P., Flerus, R., Kattner, G., Harir, M., Kanawati, B., Lucio, M., Tziotis, D., Hertkorn, N., and Gebefügi, I.: Dissolved organic matter in sea spray: a transfer study from marine surface water to aerosols, Biogeosciences, 9, 1571–1582, https://doi.org/10.5194/bg-9-1571-2012, 2012.

Schum, S. K., Zhang, B., Džepina, K., Fialho, P., Mazzoleni, C., and Mazzoleni, L. R.: Molecular and physical characteristics of aerosol at a remote free troposphere site: implications for atmospheric aging, Atmos. Chem. Phys., 18, 14017–14036, https://doi.org/10.5194/acp-18-14017-2018, 2018.

Simon, M., Dada, L., Heinritzi, M., Scholz, W., Stolzenburg, D., Fischer, L., Wagner, A. C., Kürten, A., Rörup, B., He, X.-C., Almeida, J., Baalbaki, R., Baccarini, A., Bauer, P. S., Beck, L., Bergen, A., Bianchi, F., Bräkling, S., Brilke, S., Caudillo, L., Chen, D., Chu, B., Dias, A., Draper, D. C., Duplissy, J., El-Haddad, I., Finkenzeller, H., Frege, C., Gonzalez-Carracedo, L., Gordon, H., Granzin, M., Hakala, J., Hofbauer, V., Hoyle, C. R., Kim, C., Kong, W., Lamkaddam, H., Lee, C. P., Lehtipalo, K., Leiminger, M., Mai, H., Manninen, H. E., Marie, G., Marten, R., Mentler, B., Molteni, U., Nichman, L., Nie, W., Ojdanic, A., Onnela, A., Partoll, E., Petäjä, T., Pfeifer, J., Philippov, M., Quéléver, L. L. J., Ranjithkumar, A., Rissanen, M. P., Schallhart, S., Schobesberger, S., Schuchmann, S., Shen, J., Sipilä, M., Steiner, G., Stozhkov, Y., Tauber, C., Tham, Y. J., Tomé, A. R., Vazquez-Pufleau, M., Vogel, A. L., Wagner, R., Wang, M., Wang, D. S., Wang, Y., Weber, S. K., Wu, Y., Xiao, M., Yan, C., Ye, P., Ye, Q., Zauner-Wieczorek, M., Zhou, X., Baltensperger, U., Dommen, J., Flagan, R. C., Hansel, A., Kulmala, M., Volkamer, R., Winkler, P. M., Worsnop, D. R., Donahue, N. M., Kirkby, J., and Curtius, J.: Molecular understanding of new-particle formation from α-pinene between -50 and $+25\,^{\circ}C$, At-

mos. Chem. Phys., 20, 9183–9207, https://doi.org/10.5194/acp-20-9183-2020, 2020.

Simoneit, B. R. T. and Mazurek, M. A.: Organic matter of the troposphere – II. For Part I, see Simoneit et al. (1977). Natural background of biogenic lipid matter in aerosols over the rural western united states, Atmos. Environ., 16, 2139–2159, https://doi.org/10.1016/0004-6981(82)90284-0, 1982.

Sipilä, M., Sarnela, N., Jokinen, T., Henschel, H., Junninen, H., Kontkanen, J., Richters, S., Kangasluoma, J., Franchin, A., Peräkylä, O., Rissanen, M. P., Ehn, M., Vehkamäki, H., Kurten, T., Berndt, T., Petäjä, T., Worsnop, D., Ceburnis, D., Kerminen, V.-M., Kulmala, M., and O'Dowd, C.: Molecular-scale evidence of aerosol particle formation via sequential addition of HIO3, Nature, 537, 532–534, https://doi.org/10.1038/nature19314, 2016.

Stevanović, K. Z., Bubanja, I. N. M., and Stanisavljev, D. R.: Is Iodine Oxidation with Hydrogen Peroxide Coupled with Nucleation Processes?, J. Phys. Chem. C, 123, 16671–16680, https://doi.org/10.1021/acs.jpcc.9b02563, 2019.

Tsukamoto, D., Shibano, M., and Kusano, G.: Studies on the Constituents of Broussonetia Species X. Six New Alkaloids from Broussonetia kazinoki SIEB, Chem. Pharm. Bull., 49, 1487–1491, https://doi.org/10.1248/cpb.49.1487, 2001.

Vaattovaara, P., Huttunen, P. E., Yoon, Y. J., Joutsensaari, J., Lehtinen, K. E. J., O'Dowd, C. D., and Laaksonen, A.: The composition of nucleation and Aitken modes particles during coastal nucleation events: evidence for marine secondary organic contribution, Atmos. Chem. Phys., 6, 4601–4616, https://doi.org/10.5194/acp-6-4601-2006, 2006.

VanMiddlesworth, F., Giacobbe, R. A., Lopez, M., Garrity, G., Bland, J., Bartizal, K., Fromtling, R. A., Polishook, J., Zweerink, M., and Edison, A. M.: Sphingofungins A, B, C, and D; a new family of antifungal agents. I. Fermentation, isolation, and biological activity, J. Antibiot., 45, 861–867, 1992.

Vereecken, L., Glowacki, D. R., and Pilling, M. J.: Theoretical Chemical Kinetics in Tropospheric Chemistry: Methodologies and Applications, Chem. Rev., 115, 4063–4114, https://doi.org/10.1021/cr500488p, 2015.

Volkman, J. K., Barrett, S. M., Dunstan, G. A., and Jeffrey, S. W.: C30–C32 alkyl diols and unsaturated alcohols in microalgae of the class Eustigmatophyceae, Org. Geochem., 18, 131–138, https://doi.org/10.1016/0146-6380(92)90150-V, 1992.

Wang, Y., Riva, M., Xie, H., Heikkinen, L., Schallhart, S., Zha, Q., Yan, C., He, X.-C., Peräkylä, O., and Ehn, M.: Formation of highly oxygenated organic molecules from chlorine-atom-initiated oxidation of alpha-pinene, Atmos. Chem. Phys., 20, 5145–5155, https://doi.org/10.5194/acp-20-5145-2020, 2020.

Willoughby, A. S., Wozniak, A. S., and Hatcher, P. G.: Detailed Source-Specific Molecular Composition of Ambient Aerosol Organic Matter Using Ultrahigh Resolution Mass Spectrometry and 1H NMR, Atmosphere, 7, 79, https://doi.org/10.3390/atmos7060079, 2016.

Wilson, T. W., Ladino, L. A., Alpert, P. A., Breckels, M. N., Brooks, I. M., Browse, J., Burrows, S. M., Carslaw, K. S., Huffman, J. A., Judd, C., Kilthau, W. P., Mason, R. H., McFiggans, G., Miller, L. A., Nájera, J. J., Polishchuk, E., Rae, S., Schiller, C. L., Si, M., Temprado, J. V., Whale, T. F., Wong, J. P. S., Wurl, O., Yakobi-Hancock, J. D., Abbatt, J. P. D., Aller, J. Y., Bertram, A. K., Knopf, D. A., and Murray, B. J.: A marine biogenic source of atmospheric ice-nucleating particles, Nature, 525, 234–238, https://doi.org/10.1038/nature14986, 2015.

Wu, C. H., Yang, J., Fu, Q., Zhu, B., Ruan, T., and Jiang, G. B.: Molecular characterization of water-soluble organic compounds in $PM_{2.5}$ using ultrahigh resolution mass spectrometry, Sci. Total. Environ., 668, 917–924, https://doi.org/10.1016/j.scitotenv.2019.03.031, 2019.

Xie, Q., Su, S., Chen, S., Xu, Y., Cao, D., Chen, J., Ren, L., Yue, S., Zhao, W., Sun, Y., Wang, Z., Tong, H., Su, H., Cheng, Y., Kawamura, K., Jiang, G., Liu, C.-Q., and Fu, P.: Molecular characterization of firework-related urban aerosols using Fourier transform ion cyclotron resonance mass spectrometry, Atmos. Chem. Phys., 20, 6803–6820, https://doi.org/10.5194/acp-20-6803-2020, 2020.

Yang, Y. J., Peng, Y. E., Chang, Q., Dan, C. H., Guo, W., and Wang, Y. X.: Selective Identification of Organic Iodine Compounds Using Liquid Chromatography–High Resolution Mass Spectrometry, Anal. Chem., 88, 1275–1280, https://doi.org/10.1021/acs.analchem.5b03694, 2016.

Yao, L., Wang, M.-Y., Wang, X.-K., Liu, Y.-J., Chen, H.-F., Zheng, J., Nie, W., Ding, A.-J., Geng, F.-H., Wang, D.-F., Chen, J.-M., Worsnop, D. R., and Wang, L.: Detection of atmospheric gaseous amines and amides by a high-resolution time-of-flight chemical ionization mass spectrometer with protonated ethanol reagent ions, Atmos. Chem. Phys., 16, 14527–14543, https://doi.org/10.5194/acp-16-14527-2016, 2016.

Yassine, M. M., Harir, M., Dabek, E., and Schmitt-Kopplin, P.: Structural characterization of organic aerosol using Fourier transform ion cyclotron resonance mass spectrometry: Aromaticity equivalent approach, Rapid. Commun. Mass. Sp., 28, 2445–2454, https://doi.org/10.1002/rcm.7038, 2014.

Yoon, Y. J., O'Dowd, C. D., Jennings, S. G., and Lee, S. H.: Statistical characteristics and predictability of particle formation events at Mace Head, J. Geophys. Res., 111, D13204, https://doi.org/10.1029/2005JD006284, 2006.

Yu, H.: Organic Compounds Dataset Detected by High Resolution Mass Spectrometer in Ambient Aerosols from the Coastal Atmosphere of Zhejiang, China [DB/J], Global Change Data Repository, https://doi.org/10.3974/geodb.2020.03.26.V1, 2020.

Yu, H., Ren, L., Huang, X., Xie, M., He, J., and Xiao, H.: Iodine speciation and size distribution in ambient aerosols at a coastal new particle formation hotspot in China, Atmos. Chem. Phys., 19, 4025–4039, https://doi.org/10.5194/acp-19-4025-2019, 2019.

Yvon, S. A., Saltzman, E. S., Cooper, D. J., Bates, T. S., and Thompson, A. M.: Atmospheric sulfur cycling in the tropical Pacific marine boundary layer (12° S, 135° W): A comparison of field data and model results: 1. Dimethylsulfide, J. Geophys. Res.-Atmos., 101, 6899–6909, https://doi.org/10.1029/95JD03356, 1996.

Zhao, R., Kenseth, C. M., Huang, Y., Dalleska, N. F., Kuang, X. M., Chen, J., Paulson, S. E., and Seinfeld, J. H.: Rapid Aqueous-Phase Hydrolysis of Ester Hydroperoxides Arising from Criegee Intermediates and Organic Acids. J. Phys. Chem. A, 122, 5190–5201, https://doi.org/10.1021/acs.jpca.8b02195, 2018a.

Zhao, R., Kenseth, C. M., Huang, Y., Dalleska, N. F., and Seinfeld, J. H.: Iodometry-assisted liquid chromatography electrospray ionization mass spectrometry for analysis of organic peroxides – an application to atmospheric secondary organic aerosol, Environ. Sci. Technol., 52, 2108–2117, 2018b.

Zhao, Y., Hallar, A. G., and Mazzoleni, L. R.: Atmospheric organic matter in clouds: exact masses and molecular formula identification using ultrahigh-resolution FT-ICR mass spectrometry, Atmos. Chem. Phys., 13, 12343–12362, https://doi.org/10.5194/acp-13-12343-2013, 2013.

Zheng, M., Fang, M., Wang, F., and To, K. L.: Characterization of the solvent extractable organic compounds in $PM_{2.5}$ aerosols in Hong Kong, Atmos. Environ., 34, 2691–2702, https://doi.org/10.1016/S1352-2310(99)00521-X, 2000.

Zuth, C., Vogel, A. L., Ockenfeld, S., Huesmann, R., and Hoffmann, T.: Ultrahigh-Resolution Mass Spectrometry in Real Time: Atmospheric Pressure Chemical Ionization Orbitrap Mass Spectrometry of Atmospheric Organic Aerosol, Anal. Chem., 90, 8816–8823, https://doi.org/10.1021/acs.analchem.8b00671, 2018.